EINDHOVEN UNIVERSITY OF TECHNOLOGY

Deposition of TiN and HfO2 in a commercial 200 mm remote plasma atomic layer deposition reactor

Citation for published version (APA):
Heil, S. B. S., Hemmen, van, J. L., Hodson, C. J., Singh, N., Klootwijk, J. H., Roozeboom, F., Sanden, van de, M. C. M., & Kessels, W. M. M. (2007). Deposition of TiN and HfO2 in a commercial 200 mm remote plasma atomic layer deposition reactor. *Journal of Vacuum Science and Technology A: Vacuum, Surfaces, and Films*, *25*(5), 1357-1366. https://doi.org/10.1116/1.2753846

DOI:
10.1116/1.2753846

Document status and date:
Published: 01/01/2007

Document Version:
Publisher's PDF, also known as Version of Record (includes final page, issue and volume numbers)

Please check the document version of this publication:

• A submitted manuscript is the version of the article upon submission and before peer-review. There can be important differences between the submitted version and the official published version of record. People interested in the research are advised to contact the author for the final version of the publication, or visit the DOI to the publisher's website.
• The final author version and the galley proof are versions of the publication after peer review.
• The final published version features the final layout of the paper including the volume, issue and page numbers.

Link to publication

General rights
Copyright and moral rights for the publications made accessible in the public portal are retained by the authors and/or other copyright owners and it is a condition of accessing publications that users recognise and abide by the legal requirements associated with these rights.

• Users may download and print one copy of any publication from the public portal for the purpose of private study or research.
• You may not further distribute the material or use it for any profit-making activity or commercial gain
• You may freely distribute the URL identifying the publication in the public portal.

If the publication is distributed under the terms of Article 25fa of the Dutch Copyright Act, indicated by the "Taverne" license above, please follow below link for the End User Agreement:

www.tue.nl/taverne

Take down policy
If you believe that this document breaches copyright please contact us at:

openaccess@tue.nl

providing details and we will investigate your claim.

Download date: 22. Aug. 2022

Deposition of TiN and HfO_2 in a commercial 200 mm remote plasma atomic layer deposition reactor

S. B. S. Heil and J. L. van Hemmen
Department of Applied Physics, Eindhoven University of Technology, P.O. Box 513, 5600 MB Eindhoven, The Netherlands

C. J. Hodson and N. Singh
Oxford Instruments Plasma Technology, North End, Yatton BS49 4AP, United Kingdom

J. H. Klootwijk
Philips Research Laboratories, High Tech Campus 4, 5656 AE Eindhoven, The Netherlands

F. Roozeboom
NXP Semiconductors Research, High Tech Campus 4, 5656 AE Eindhoven, The Netherlands

M. C. M. van de Sanden and W. M. M. Kessels[a]
Department of Applied Physics, Eindhoven University of Technology, P.O. Box 513, 5600 MB Eindhoven, The Netherlands

(Received 5 March 2007; accepted 5 June 2007; published 31 July 2007)

The authors describe a remote plasma atomic layer deposition reactor (Oxford Instruments FlexAL™) that includes an inductively coupled plasma source and a load lock capable of handling substrates up to 200 mm in diameter. The deposition of titanium nitride (TiN) and hafnium oxide (HfO_2) is described for the combination of the metal-halide precursor $TiCl_4$ and H_2-N_2 plasma and the combination of the metallorganic precursor $Hf[N(CH_3)(C_2H_5)]_4$ and O_2 plasma, respectively. The influence of the plasma exposure time and substrate temperature has been studied and compositional, structural, and electrical properties are reported. TiN films with a low Cl impurity content were obtained at 350 °C at a growth rate of 0.35 Å/cycle with an electrical resistivity as low as 150 $\mu\Omega$ cm. Carbon-free (detection limit <2 at. %) HfO_2 films were obtained at a growth rate of 1.0 Å/cycle at 290 °C. The thickness and resisitivity nonuniformity was <5% for the TiN and the thickness uniformality was <2% for the HfO_2 films as determined over 200 mm wafers. © *2007 American Vacuum Society.* [DOI: 10.1116/1.2753846]

I. INTRODUCTION

From industry there is a pressing demand for high-quality thin films with decreasing thicknesses, i.e., within the range of 1 nm to a few tens of nanometers, over increasingly larger substrate areas. Often these films also need to be deposited at relatively low substrate temperatures (<400 °C) and on substrates with demanding topologies. Atomic layer deposition (ALD) is considered as the method of choice for these applications,[1] although a wide variety of technological challenges still needs to be met before large-scale implementation of this method in industry will take place. Nevertheless, ALD processing has already proven itself in production schemes for, e.g., electroluminescent displays,[2] while ALD is currently also being introduced in deep trench capacitors in dynamic random access memory at the production level.[3–5] Furthermore, ALD is at the verge of being introduced in the production of complementary metal-oxide semiconductor capacitor stacks while the application of ALD films at the interconnect level of state-of-the-art integrated circuits is actively being researched.[6] More recently, the scope of potential applications has been widened with research on ALD films rapidly emerging in fields such as flexible electronics,[7,8] photovoltaics,[9,10] photonics,[11,12] and microsystems.[13,14]

So far, most research has been concentrated on so-called thermal ALD processes, where the chemistry of the process is thermally activated due to the (elevated) deposition temperature. Also the application of ALD in industry has been limited to thermal ALD with commercial thermal ALD reactors widely available, both for research and for production purposes. A trend that started half a decade ago and that is currently gaining more momentum is the introduction of a plasma step in the ALD process. This so-called plasma-enhanced or plasma-assisted ALD has several advantages such as deposition at reduced temperatures, increased choice of precursors and materials, higher growth rate, more process versatility, and in some case also improved material properties. These advantages of plasma-assisted ALD are important for applications of ALD currently being investigated but they might turn out to be of key importance for the aforementioned emerging applications of ALD. Plasma-assisted ALD of oxides,[15–17] nitrides,[18–20] and metals[21–24] has already been demonstrated. The studies on plasma-assisted ALD have mostly been carried out in homebuilt laboratory scale reactors which are often limited to small substrate sizes. However, with the interest in plasma-assisted ALD growing, tool

[a]Author to whom correspondence should be addressed; electronic mail: w.m.m.kessels@tue.nl

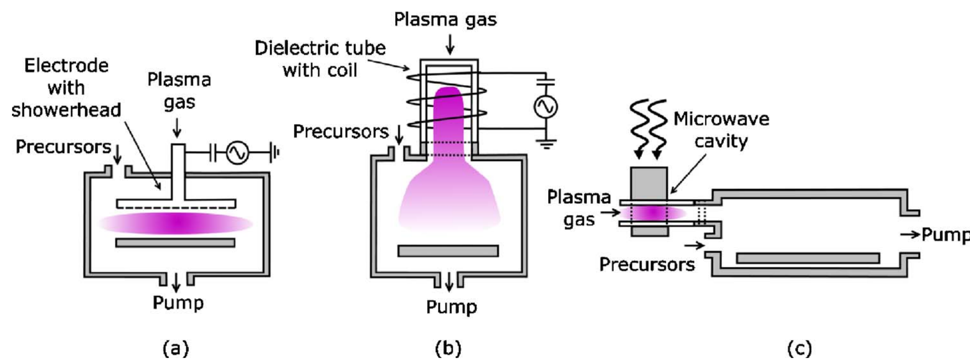

FIG. 1. Schematic representation of the three different types of plasma-assisted atomic layer deposition that can be distinguished: (a) direct plasma, (b) remote plasma, and (c) radical enhanced. For each type different hardware configurations and plasma sources exist.

manufacturers have started to work on commercial plasma-assisted ALD reactors with to date only one manufacturer reported to offer a plasma-assisted ALD reactor for production applications.[25] Most plasma-assisted ALD reactors, including the few commercial tools, are so-called *direct plasma* ALD reactors. In a direct plasma ALD reactor, plasma generation takes place in between two electrodes positioned in the ALD chamber and with the substrate mounted on one of the electrodes [cf. Fig. 1(a)]. This is a relatively simple approach that allows for a small reactor volume and flow-type operation, although layers are grown here at the cost of possible plasma damage due to the relatively high ion energies involved. Other types of plasma-assisted ALD reactors are *remote plasma* ALD [cf. Fig. 1(b)] and *radical-enhanced* ALD [cf. Fig. 1(c)], yet until recently reactors based on these configurations were not commercially available.

Remote plasmas are a well-proven concept in plasma-enhanced chemical vapor deposition (PECVD).[26] In a remote plasma reactor, the plasma creation takes place upstream of the substrate stage independently of the substrate conditions. This allows for independent optimization of the plasma properties as well as the ability to tune the chemistry of the plasma when it flows or diffuses to the substrate. The plasma species including ions and electrons are generally still in contact with the substrate; however, the energies of ions impacting the surface are well below the threshold value for ion-induced plasma damage. Under particular conditions, the mild ion energies might even have a beneficial effect on the surface chemistry as they add energy to the substrate without heating it. The contact between plasma and substrate as well as the mild ion energies distinguish remote plasma ALD from radical-enhanced ALD. In the latter configuration, plasma creation takes place at a large distance from the substrate such that the electron and ion densities in the plasma are low at the substrate region. Amongst the reactive species, only longer lived radicals are able to reach the substrate, however, generally at reduced fluxes due to wall recombination processes. Although from a hardware point of view, remote plasma ALD is still at its infancy, several studies using remote plasma ALD reactors have been reported[20,21,27,28] that all indicate that these reactors are well suited for research and development applications. Besides their mild ion bombardment, they provide a high flux of plasma species enabling relatively short plasma exposure times, while their geometry in principle also allows for a good uniformity over large substrates. Furthermore, remote plasma ALD reactors offer a high degree of versatility due to the remote plasma creation (which, e.g., also can be used for plasma cleaning), while the plasma source can also be isolated from the ALD chamber for thermal ALD studies.

In the present work, we describe the recently introduced Oxford Instruments FlexAL™ reactor, which is a remote plasma reactor that is also suited for thermal ALD. This reactor, aimed particularly at research and development studies, is equipped with a load lock and is capable of handling substrate sizes up to 200 mm in diameter. In this article, the reactor is described in detail and results obtained for both a nitride and an oxide are presented employing two different types of precursors, i.e., a metal-halide and a metal organic precursor. TiN films were deposited from $TiCl_4$ in combination with a H_2-N_2 plasma. In our previous work on a home-built laboratory scale reactor, we have also studied this process for small substrate sizes;[20] here we report on scaling up the process to substrate sizes up to 200 mm with simultaneously optimizing the cycle time of the process. Results using the same reagents have also been reported for direct plasma ALD by Elers *et al.* who showed that obtaining a good uniformity is challenging.[29,30] Furthermore, in the current study also results obtained at low substrate temperatures (temperature range is 150–350 °C) are presented, while the direct plasma ALD results were limited to temperatures above 300 °C. Films of the high-*k* dielectric HfO_2 were deposited by the metal organic precursor $Hf[N(CH_3)(C_2H_5)]_4$ [tetrakis(ethylmethylamido)hafnium (TEMAH)] in combination with an O_2 plasma. The TEMAH precursor together with the other alkylamides $Hf[N(CH_2)]_4$ [tetrakis(dimethylamido)hafnium (TDMAH)] and $Hf[N(C_2H_5)_2]_4$ [tetrakis(diethylamido)hafnium (TDEAH)] form the most commonly used metal organic precursors for thermal ALD of HfO_2.[31–34] For plasma-assisted ALD mainly the usage of TDEAH (Refs. 15 and 27) in combination with an O_2 plasma is reported and only few reports of TEMAH exist.[35] Here, we present a parameter study of the growth rate as a function of deposition temperature and plasma exposure time while also addressing material properties such as morphology, microstructure, and dielectric performance. The difference with other Hf based

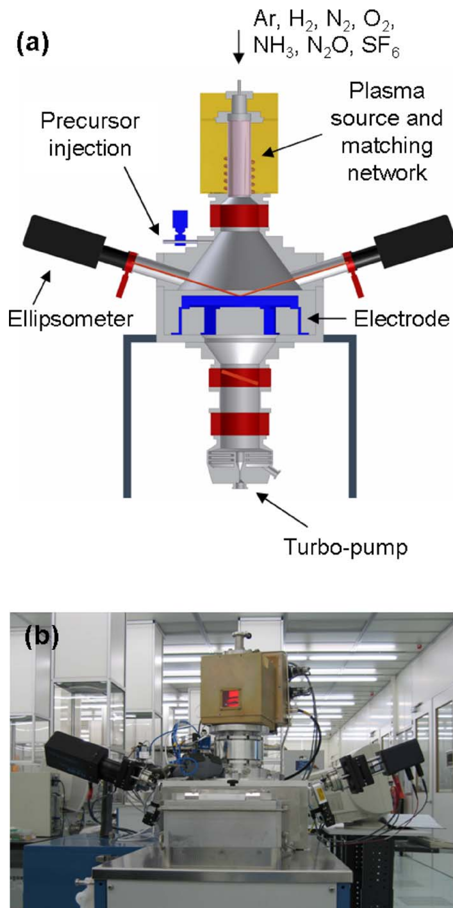

FIG. 2. (a) Schematic representation of the Oxford Instruments FlexAL reactor for remote plasma and thermal atomic layer depositions. The figure shows the main deposition chamber, the inductively coupled plasma (ICP) source, and the *in situ* spectroscopic ellipsometer. Not shown are the precursor modules and the differentially pumped mass spectrometer. (b) Photograph of the FlexAL reactor showing the load lock (front), the plasma source and matching network (top), *in situ* spectroscopic ellipsometer (at both sides), and the precursor modules (bottom left). The precursors are injected into the chamber just below the gate valve that can be used to isolate the plasma source from the chamber.

metal organic precursors and with other methods of atomic layer deposition is briefly discussed. Furthermore, it is noted that the deposition of Al_2O_3 by remote plasma ALD and thermal ALD in the FlexAL™ reactor will be addressed in a separate publication.[36]

II. EXPERIMENT

A. FlexAL reactor

In Fig. 2, a schematic of the Oxford Instruments FlexAL reactor is given.[37] The reactor consists of a main deposition chamber to which a pump unit, a plasma source, and a load lock are connected through gate valves.

The aluminum deposition chamber is optimized to minimize the volume and the presence of dead spaces while maintaining a good film uniformity and pumping capacity. A 240 mm diameter ceramic heater is located in the center of the deposition chamber and its temperature can be actively controlled between 25 and 400 °C. The chamber wall temperature can be controlled separately between room temperature and a maximum temperature of 120 °C.

A base pressure of $\sim 10^{-6}$ Torr in the chamber is reached by a nitrogen-purged 400 l/s turbo molecular pump which is backed by a Fomblin oil greased rotary vane pump. The operating pressure in the chamber during processing can be set using an automated pressure controller (APC), which comprises a fast (90 ms open-close) butterfly valve located in front of the turbo pump and a 100 mTorr capacitance manometer gauge mounted on the chamber. A gate valve is positioned in between the APC and the turbo pump to isolate the pump from the chamber (e.g., for the case of venting to atmosphere). The valves, the piping in between, and the turbo pump itself are heated to prevent precursor condensation. Also the exhaust line between the turbo pump and the foreline pump is heated.

The plasma is generated by a remotely placed inductively coupled plasma source operating at a pressure of typically 10 mTorr. The source can deliver up to 600 W of radio frequency power at 13.56 MHz and is controlled by an automated matching network. The source consists of a three turn water-cooled copper coil around a 65 mm Al_2O_3 ceramic plasma tube. A wide range of gases such as Ar, H_2, N_2, O_2, NH_3, SF_6, and N_2O is connected to a common plasma source line. The flow of the plasma source gases is controlled by dedicated mass flow controllers (maximum range is 500 SCCM for Ar, 100 SCCM for H_2, N_2, O_2, SF_6, and N_2O, and 50 SCCM for NH_3) (SCCM denotes cubic centimeter per minute at STP) located in an extractable gas cabinet. There is no special gas mixing besides in the plasma source line when two or more source gases are used simultaneously. The source gases are fed axially into the plasma tube and the plasma-generated radicals diffuse through the 100 mm gate valve into the deposition chamber. When depositing conductive films the gate valve is closed during the precursor dosing to prevent film deposition inside the source. When using the reactor for thermal ALD, the gate valve can also remain closed and the reducing or oxidizing gases can directly be injected into the chamber.

Liquid and solid precursors can be delivered into the process chamber from bubbler source pots sited in independently heated and extracted modules close to the deposition chamber. The precursor delivery module and delivery lines from the module to the process chamber are heated. Precursors are delivered into the chamber by fast ALD valves with a minimum opening time of 10 ms. The precursors are injected into the deposition chamber above the center of the substrate stage through a cone-shaped flange positioned just below the gate valve to the plasma source. Depending on the vapor pressure of the precursor at the set temperature, the delivery can be either vapor drawn or via bubbling with ultrapure Ar carrier gas. In the case of bubbling the Ar gas is diverted directly into the deposition chamber when no precursor dosing takes place. The use of a divert line ensures fast on and off switching of the precursor without the need of very fast acting mass flow controllers. Moreover, when di-

verted, the Ar acts as purge gas. In the precursor module a cross valve is positioned between the gas line where the Ar gas enters the bubbler and the exit line to the deposition chamber. This enables extensive purging of the precursor lines after bubbler exchange. Furthermore, the precursor delivery lines and ALD valves are separately heated and are set to a temperature generally 10–20 °C higher than the precursor module to prevent condensation of the precursors in the lines.

Substrates are transferred into the deposition chamber using a load lock. The load lock is separately pumped with a base pressure of 10^{-5} Torr and can directly transfer wafer sizes ranging from 50 to 200 mm in diameter, while other substrate sizes and shapes require the use of a carrier wafer.

The reactor operation is completely automated and computer controlled. In a graphical user interface different menus exist for setting process recipes. Standard recipes such as SF_6 plasma cleaning for the removal of, for example, TiN film residues on the chamber walls are also available.

Diagnostic ports located at 70° with the normal on the substrate stage allow *in situ* ellipsometry measurements for online measurements of the thickness and film optical properties.[38] The windows are valved off when not in use. An additional analytical port positioned above the wafer may be used for residual gas analysis using a differentially pumped quadrupole mass spectrometer. As shown earlier by our group, these analytical capabilities allow for fast process development and process condition monitoring.[39,40]

B. Details on TiN and HfO_2 deposition

For the TiN depositions, titanium tetrachloride (99.995 +%, Sigma-Aldrich, $TiCl_4$) contained in a glass flask, kept at room temperature, is vapor drawn into the setup using a fixed open-close time of the ALD valve of 40 ms. The plasma is generated in a H_2–N_2 (both purity >99.999%) gas mixture in a ratio of ~10:1 to produce N, H, and NH_x radical species, etc., to remove the chlorine from the surface and nitridate the film. For the deposition of HfO_2, tetrakis(ethylmethylamido)hafnium (99.99+%, Sigma-Aldrich, TEMAH) contained in a stainless steel bubbler, heated to 70 °C, is bubbled using a 30 SCCM Ar (purity >99.9999%) flow for a variable dosing period. The plasma is generated in O_2 (purity >99.999%) gas to produce O radicals that are considered to be the main oxidizing species.

The TiN and HfO_2 films were deposited on 200 mm *p*-type monocrystalline Si (100) wafers with a resistivity of 10–30 Ω cm. Unless otherwise mentioned, the wafers were not additionally cleaned and therefore an ~2 nm native oxide layer was present. For electrical characterization some HfO_2 films were grown on boron doped *p*-type monocrystalline Si substrates (~1 Ω cm), which were dipped in a diluted HF solution (1% HF) for 1 min and rinsed with de-ionized water prior to deposition.

C. Analysis techniques

For studying the TiN film growth, a visible to near-infrared (245–1700 nm) spectroscopic ellipsometer (J.A. Woollam, Inc. M2000U) was used for *in situ* thickness measurements. The data were analyzed using a Drude-Lorentz oscillator model as described in Ref. 38. For the HfO_2 depositions, an ultraviolet to visible (190–1000 nm) ellipsometer (J.A. Woollam, Inc. M2000D) was used. In this case the data were analyzed by a Tauc-Lorentz oscillator model. Thickness uniformity measurements were performed by *ex situ* spectroscopic ellipsometry using the aforementioned ellipsometers or by optical reflectivity using a Nanometrics Nanospec 3000 series (~300–800 nm).

The film composition was determined by Rutherford backscattering spectrometry (RBS) using a 2 MeV $^4He^+$ beam under an 80° angle for determining the Hf, Ti, N, O, Cl, and C areal densities of the films. Using the same beam settings, also elastic recoil detection (ERD) measurements were performed for determining the H areal density. Atomic densities and concentrations were calculated from the areal densities using the thickness data obtained by spectroscopic ellipsometry.

The structure of the deposited films was studied using a Panalytical/Philips X'Pert Pro MPD diffractometer equipped with a Cu $K\alpha$ x-ray source and an X'Celerator detector. An ordinary 2θ-ω scan has been performed in the analysis of the HfO_2 samples. A grazing incidence measurement under 0.32° incidence angle for high surface sensitivity has been performed on the TiN samples.

Resistivity measurements were performed *ex situ* and at room temperature using a Signatone four-point probe in combination with a Keithley 2400 Sourcemeter acting both as a current source and as a voltage meter. The resistivity of the TiN films was determined from the slope of the *I-V* curve. Capacitance-voltage (*C-V*) measurements were performed to characterize the HfO_2 dielectric properties. Circular Al contacts with sizes ranging from 0.02 to 1.2 mm^2 were sputter deposited at room temperature using a shadow mask; the wafer back side served as the bottom electrode. The dielectric constant of the HfO_2 films after forming gas anneal (30 min, 425 °C, 10% H_2–90% N_2) was determined by 10 kHz *C-V* measurements with an HP4275A multifrequency *LCR* meter and an Agilent 4155B parameter analyzer.

III. RESULTS AND DISCUSSION

A. TiN

In Fig. 3 a schematic of the ALD cycle for TiN is shown. At the start of the cycle a continuous Ar flow (150 SCCM) is run through the chamber and the pressure is set to 80 mTorr. $TiCl_4$ kept at room temperature is dosed into the vessel by opening the ALD valve for typically $t_{precursor}$=40 ms. After dosing, the Ar flow serves as a purge gas (t_{Ar}=3 s). Subsequently, the valve in between the plasma source and chamber is opened and Ar flow is switched off. At the same time a H_2–N_2 flow (30 and 4 SCCM for H_2 and N_2, respectively) is

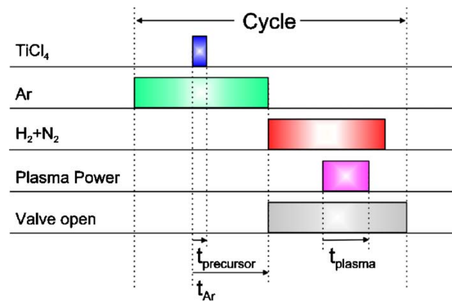

FIG. 3. Schematic layout of the cycle for remote plasma ALD of TiN in which $TiCl_4$ is used as precursor and H_2-N_2 as plasma gas. Ar is used for purging of the chamber. The switching of the plasma power and the gate valve between plasma source and deposition chamber is also shown.

set through the plasma source and when the pressure stabilizes at 15 mTorr the plasma is ignited (t_{plasma}). Shortly after the plasma power (250 W) is switched off, when the reaction products are pumped out, the H_2-N_2 flow is switched off, the valve is closed again, and an Ar flow is initiated for the next cycle.

In Table I an overview of the TiN deposition conditions, process properties, and resulting material properties is given. There are two series in which the varied parameters are the plasma exposure time and the deposition temperature. For the plasma series the temperature was kept constant at 350 °C, and the cycle time varied from 11 to 29 s. The selected "standard" deposition condition (sample BT28) is shown for both series. The 40 ms dosing with $TiCl_4$ proved sufficient to reach saturating conditions both in growth rate and uniformity across the substrate at all given temperatures, as will be discussed below.

Figure 4(a) shows that the growth rate saturates at ~0.4 Å/cycle at 350 °C for plasma exposures larger than 5 s. For the temperature series, a plasma exposure of 10 s was therefore selected, resulting in a cycle time of 19 s. Figure 4(b) shows a decrease of the growth rate when operating at a lower deposition temperature. This is similar to what we have observed before for depositions carried out in a smaller laboratory scale reactor, here referred to as "ALD-I." These data which were obtained previously are also shown in Fig. 4(b) for comparison.[20] It can be observed that the growth rate at 350 °C is slightly lower, 0.39 Å/cycle, than the trend on the basis of the ALD-I results would suggest. This minor

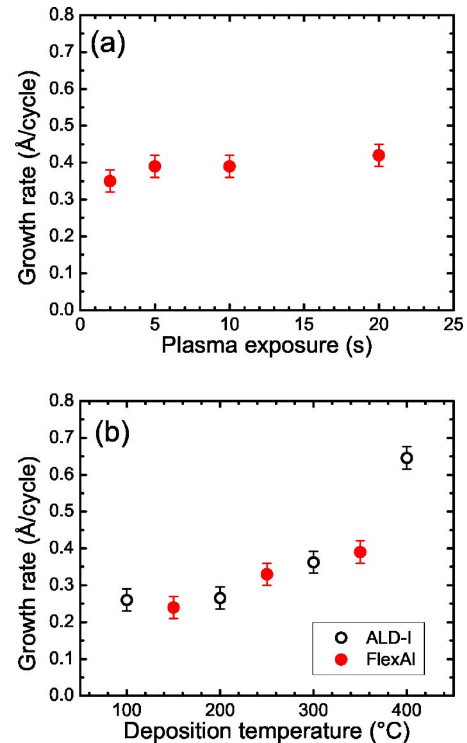

FIG. 4. Growth rate per cycle as a function of (a) the H_2-N_2 plasma exposure time at 350 °C and (b) the substrate temperature using a H_2-N_2 plasma exposure time of 10 s. For comparison, in (b) also the growth rate per cycle as obtained in the homebuilt laboratory scale reactor "ALD-I" is given (Ref. 20).

TABLE I. Overview of the TiN deposition conditions and film analysis results from Rutherford backscattering spectrometry (RBS), spectroscopic ellipsometry (SE), and four-point probe measurements (FPP) performed at the center of the substrate. The mass density is calculated by combining the RBS and SE results. The first row gives the typical absolute errors in the parameters.

			Analysis results						
			RBS			SE			
Sample	T_{dep} (°C)	t_{plasma} (s)	TiN_x	Cl (at. %)	O (at. %)	Thickness (nm)	Growth rate Å/cycle	FPP resistivity (μΩ cm)	Mass density (g cm^{-3})
Plasma series									
BT29	350	2	0.93±0.02	2.7±0.1	2.0±0.1	21.1±0.2	0.35±0.02	175±15	4.0±0.1
BT27	350	5	0.93	1.8	2.0	23.2	0.39	162	3.9
BT28	350	10	0.93	1.3	2.0	23.5	0.39	147	4.0
BT30	350	20	⋯	⋯	⋯	25.2	0.42	145	
Temperature series									
BT28	350	10	0.93	1.3	2.0	23.5	0.39	147	4.0
BT35	250	10	0.95	6.0	4.0	19.8	0.33	362	3.9
BT36	150	10	0.95	14.6	4.0	14.4	0.24	1624	3.4

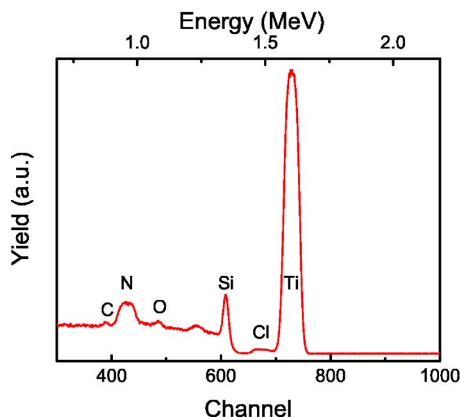

FIG. 5. Typical Rutherford backscattering spectrum of a remote plasma ALD TiN film (BT28, 23.5 nm thick) deposited on a crystalline Si substrate.

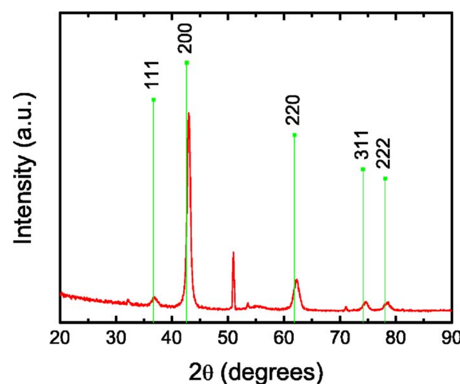

FIG. 6. Typical grazing incidence x-ray diffractogram of a remote plasma ALD TiN film (BT28, 23.5 nm thick). The peak positions and relative intensities of the different crystallographic planes for a randomly oriented TiN powder sample have been indicated. The nonlabeled peaks originate from the crystalline Si substrate.

discrepancy can most probably be explained by a small difference, 10–15° C in actual wafer surface temperature between the ALD-I and the FlexAL reactors. Slightly different growth rates, however, have been reported for various types of reactors and for different plasma composition and power settings.[29,41]

As is shown by the RBS results in Table I, the films are slightly Ti rich with the ratio $[N]/[Ti]=0.93-0.95$ for all deposition conditions. Contrary to what was observed before,[20] in this case the plasma exposure time did not show to have an influence on the stoichiometry. Cl and O impurities were found to be present throughout the film, as can be clearly observed in Fig. 5. The Cl content is found to be reduced when longer plasma exposure times are used at 350 °C. A dramatic increase in Cl content, however, occurs when using lower deposition temperatures. The Cl content rises from 1.3 at. % at 350 °C to 14.6 at. % at 150 °C. Similar results have been reported before for both thermal and plasma-assisted ALDs at 350 °C. However, in the ALD-I setup we managed to have lower Cl impurities as low as ~7 at. % at a deposition temperature of 100 °C by extending the plasma exposure time to 30 s.[20] It appears that in this larger reactor also longer plasma exposures are required at low temperatures to sufficiently reduce the impurity contents.

Figure 6 shows an x-ray diffraction (XRD) spectrum of the TiN film deposited under standard conditions, 350 °C, 10 s plasma exposure. The diffractogram contains peaks originating from crystalline TiN, of which the expected peak positions are indicated by the reference pattern. All other peaks that are visible originate from the Si substrate. The TiN peaks are at slightly higher diffraction angle than the positions of the reference pattern. This indicates a slightly smaller lattice constant, which might be due to the nitrogen deficiency, which was also observed in the RBS measurements, or due to (tensile) stress in the TiN layer. The ordinary 2θ-ω measurement yielded only one TiN diffraction peak, the [2 0 0] peak between 42° and 43°. This indicates a preferred orientation of the TiN crystallites, with their (2 0 0) lattice planes parallel to the sample surface. This has been observed before for TiN deposition by various techniques and appeared to be mainly deposition temperature dependent, lower temperatures typically resulting in films with a polymorphous or amorphous structure.[20]

The electrical properties of the film can be improved by extending the plasma exposure, as can be observed in Fig. 7. For a plasma exposure longer than 10 s at 350 °C, the resistivity seems to level off at ~145 $\mu\Omega$ cm for 25 nm thick films. The resistivity, however, becomes very high, when going to lower deposition temperatures, 1624 ± 15 $\mu\Omega$ cm at 150 °C. This is most probably due to the scattering of the carrier electrons at Cl impurities (14.6 at. %). This was indicated by the electron mean free path being decreased as the Cl content increases, which was observed before by spectroscopic ellipsometry.[38] The resistivity could be improved by extending the plasma exposure resulting in a reduction of Cl content,[20] but this option has not been pursued in the current study.

In Fig. 8 the thickness and resistivity uniformity of a TiN film (5 s plasma exposure, 12–13 nm thickness) is plotted. The nonuniformity as defined by (maximum-minimum)/(2 $\times$ average) was 5% using an edge exclusion of 10 mm. No correlation between the precursor injection position and the

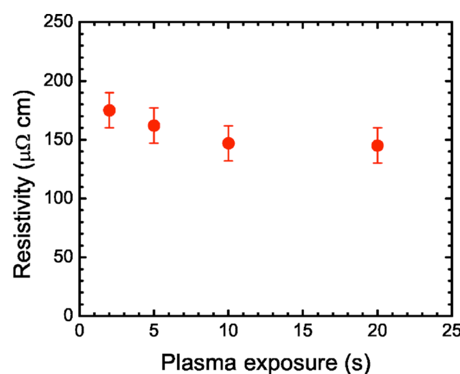

FIG. 7. Resistivity as a function of the plasma exposure time for 20–25 nm thick TiN films deposited at a temperature of 350 °C.

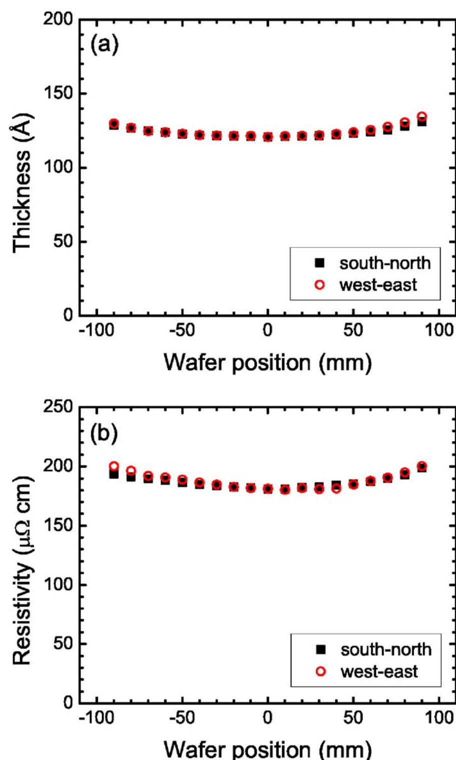

FIG. 8. Uniformity across the wafer centerline of (a) thickness and (b) resistivity as measured by spectroscopic ellipsometry and four-point probe, respectively. The 12 nm (nominal) thick film was deposited at 350 °C using a 5 s plasma exposure time.

profile was observed, indicating that the symmetric "bowl" shape is solely due to the radical profile. Since most remote plasma reactors are small homebuilt systems, no literature comparison is available for such large wafer diameter. A similar uniformity profile can also be observed for the resistivity in Fig. 8(b).

As stated earlier, details about the (non)uniformity of deposition over the substrate area have hardly been reported. However, uniformity is an important factor in the scalability of direct, remote plasma, and radical-enhanced based ALD processes. In a recent review, Elers *et al.* pointed out that the most typical reasons for nonuniformity are considered to be overlapping material pulses, nonuniform gas distribution, and thermal self-decomposition of the precursor.[30] Reactor design and plasma operation were also found to play a key role in the deposition of TiN from $TiCl_4$ and a direct H_2-N_2 plasma using a showerhead gas distributor.[29] In this fashion a uniformity of 1%–3% was obtained over 300 mm wafers. We would like to note here that with considerably less design effort, in terms of reactor optimization, we already obtained a fair resistivity uniformity of <5% suitable for most research environments.

The material properties for TiN obtained in the FlexAL reactor in terms of resistivity, microstructure, and surface morphology were found to be comparable to the results reported earlier by our group for using the same $TiCl_4$ and H_2-N_2 plasma chemistry in the homebuilt ALD-I reactor[20] and by Elers *et al.* for the direct plasma showerhead reactor[29]

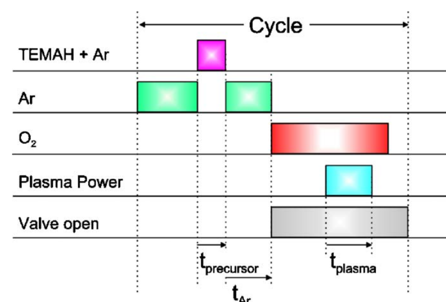

FIG. 9. Schematic of the remote plasma ALD cycle for deposition of HfO_2. $Hf[N(CH_3)(C_2H_5)]_4$ (TEMAH) is used as precursor and O_2 as plasma gas. Ar is used for purging of the chamber and bubbling the TEMAH. The switching of the plasma power and the gate valve between plasma source and deposition chamber is also shown.

for temperatures above 300 °C. For low deposition temperatures the results look moderate but with room for improvement. This indicates a successful transfer and upscaling of the process from the small remote plasma ALD reactor to the FlexAL reactor.

B. HfO_2

In Fig. 9 the ALD cycle for the HfO_2 deposition is given. The valve between the plasma source and chamber is closed during the precursor injection and purging. The Ar flow (150 SCCM) is injected directly into the chamber for purging (80 mTorr) or is diverted through the TEMAH containing bubbler which is kept at 70 °C. Typically, the dosing time is $t_{precursor}=1$ s. After the purge, $t_{Ar}=2$ s, the top valve is opened and an O_2 flow is started through the source. The plasma power (250 W) is turned on after 2 s, when the O_2 flow is stabilized and a pressure of 10 mTorr is reached. After the plasma exposure ($t_{plasma}=3$ s), the valve is closed again. The Ar flow is switched on for the next cycle.

In Table II the deposition conditions, process characteristics, and resulting material properties of the HfO_2 films are presented. Similar to the TiN case, here also the plasma exposure time and deposition temperature are the parameters varied and the selected standard condition (PH88) is present in both series. The dosing time of 1 s bubbling proved sufficient to deliver a saturated dose of TEMAH at all temperatures.

As can be observed in Fig. 10, the growth appears to be constant around 1.0 Å/cycle for all plasma exposure times. In an attempt to keep the cycle times as short as possible, a 3 s plasma exposure was chosen for the temperature series, which resulted in a cycle time of 11 s. The growth rate appears to be fairly constant in the temperature range of 230–350 °C, showing a little decrease going to higher temperatures. Decreasing growth rates with temperature have been found to be common to (plasma-assisted) ALD processes of oxides and have also been observed for, e.g., Al_2O_3 and ZrO_2.[36,40,42,43] The decrease in growth rate is suggested to be due to a decrease in reactive surface sites such as surface hydroxyl groups (–OH) by dehydroxylation.

TABLE II. Overview of the HfO_2 deposition conditions and film analysis results from Rutherford backscattering spectrometry (RBS) and spectroscopic ellipsometry (SE) performed at the center of the substrate. The mass density is calculated by combining the RBS and SE results. The first row gives the typical absolute errors in the parameters.

			Analysis results					
			RBS			SE		
Sample	T_{dep} (°C)	t_{plasma} (s)	HfO_x	H (at. %)	C (at. %)	Thickness (nm)	Growth rate (Å/cycle)	Mass density (g cm^{-3})
Plasma series								
PH88	290	3	2.1±0.02	3.4±0.2	<2±0.2	41.1±0.2	1.03±0.02	9.6±0.1
PH65	290	5	2.1	1.9	<2	30.4	1.01	9.3
PH69	290	20	2.1	0.6	<2	30.0	1.00	9.7
Temperature series								
PH90	350	3	2.0	1.6	<2	40.5	1.01	10.0
PH88	290	3	2.1	3.4	<2	41.1	1.03	9.6
PH92	230	3	2.2	13	<2	42.1	1.05	7.3

RBS analysis shows that the films are close to stoichiometric and for almost all depositions the carbon content was below the detection limit of 2 at. %, which for RBS is dictated by the cracking of hydrocarbon species at the film surface during measurement. A typical RBS spectrum of a 40 nm HfO_2 film (PH88) in which C, O, and Hf have been indicated is shown in Fig. 11. More apparent, however, is the trend in hydrogen content in the films with temperature as measured by ERD. There is a considerable amount, 13 at. %, of hydrogen present in the film at the lowest deposition temperature of 230 °C. We assume that the hydrogen is mainly incorporated in the form of OH bonds. The mass density as determined from the RBS aerial density and the SE thickness measurements showed an increase in density with plasma exposure time and deposition temperature approaching the bulk density of HfO_2 (9.68 g cm^{-3}) under the best conditions.

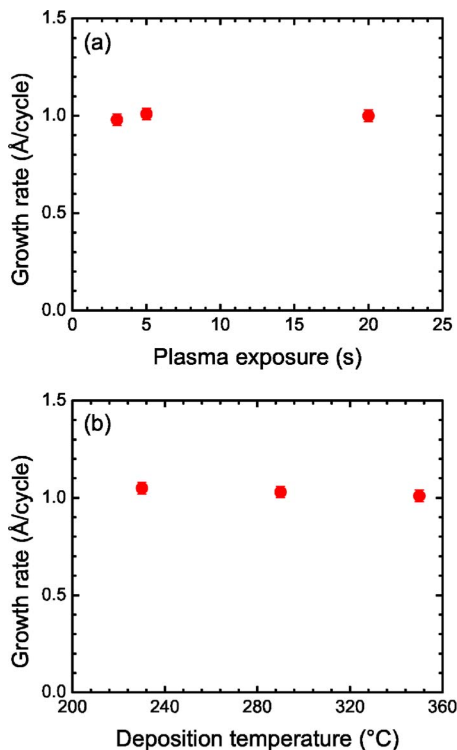

FIG. 10. Growth rate as a function of (a) the plasma exposure time at 290 °C and (b) the deposition temperature using a 3 s plasma exposure.

In Fig. 12 a typical XRD diffractrogram for a 40 nm HfO_2 film is shown. The large peak at $\theta=69°$ is due to the Si substrate; all other substrate peaks were suppressed by rotating the substrate. The small structure observed at $\theta=30°$ is due to an amorphous HfO_2 film being present on the crystalline Si substrate. Although for thermal ALD processes using the $HfCl_4$ precursor and H_2O as oxidant the presence of the monoclinic phase of HfO_2 is commonly reported,[44] the use of a metal organic precursor in both remote plasma-assisted and thermal ALDs typically resulted in the deposition of amorphous films.[27,31,33,34]

The thickness nonuniformity is given in Fig. 13 and is <2% for a 200 mm wafer and <1% for 100 mm and smaller substrates. Both Nanospec and spectroscopic ellipsometry

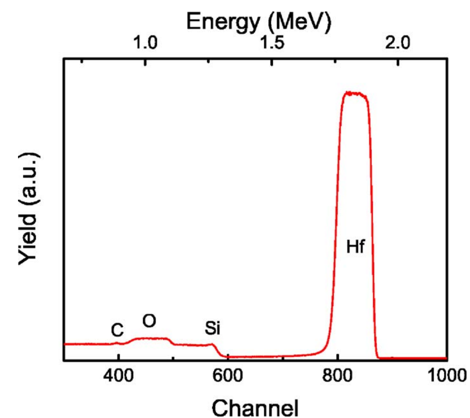

FIG. 11. Typical Rutherford backscattering spectrum for a remote plasma ALD HfO_2 film (PH88, 41.1 nm thick) deposited on a crystalline Si substrate.

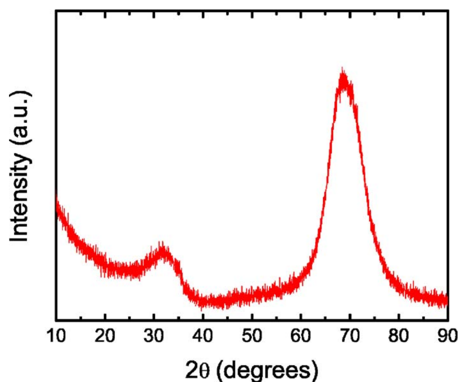

FIG. 12. Typical x-ray diffractogram for a remote plasma ALD HfO_2 film (PH90, 40 nm thick). The small structure at $\theta = \sim 30°$ is due to amorphous HfO_2. The large peak at $\theta = 69°$ is due to the crystalline Si substrate.

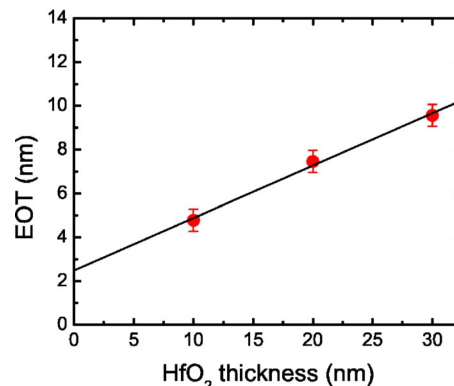

FIG. 14. Equivalent oxide thickness (EOT) of HfO_2 films derived from *C-V* measurements vs physical thickness measured by spectroscopic ellipsometry.

(SE) thickness measurements show similar results for the uniformity. In contrast to the TiN depositions no apparent bowl-shaped profile was observed. We suggest this difference to be related to the different chemistries between the O_2 and H_2-N_2 plasmas in which the relatively long lifetime of oxygen radicals compared to the radicals generated in the H_2-N_2 plasma possibly plays a role.

For the electrical characterization, HfO_2 films with three different film thicknesses were grown, using 100, 200, and 300 cycles. The results of *C-V* measurements are shown in Fig. 14, where the equivalent oxide thickness (EOT) is plotted versus the physical thickness as measured by spectroscopic ellipsometry. The annealed samples showed a clear trend with thickness and a k value of 16.3 could be extracted from a linear fit of the EOT values with physical thickness.[36] The offset in the fit through the annealed samples possibly indicates the presence of a SiO_x interfacial layer between the HfO_2 film and the substrate.

The k value of the films deposited here ($k \sim 16.3$) is close to the range of what is typically reported ($k \sim 17-18$) for different types of plasma-assisted ALD (Ref. 27) and thermal ALD.[45] The deposition temperature and annealing method, however, seem to be the key in tuning the microstructure of the HfO_2 film, which is the main factor determining the resulting k value and leakage current.[27,46] The presence of a crystalline part of the HfO_2 film gives rise to a higher dielectric constant, while the amorphous part is considered to be a better barrier for leakage current. The optimization of parameters leading to a desirable microstructure has not been pursued here but will be part of future work.

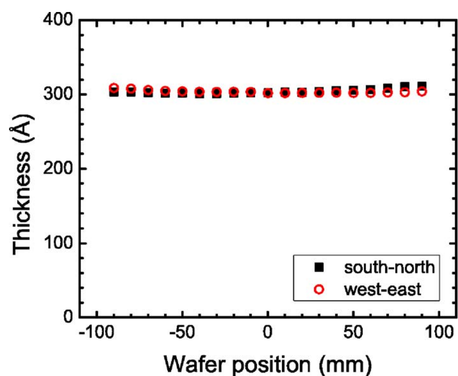

FIG. 13. Thickness uniformity of a HfO_2 film across the wafer centerline as obtained by Nanospec measurements.

The growth rate of 1.0 Å/cycle is slightly higher to what has been typically reported for thermal based processes using TEMAH and H_2O, 0.8–0.9 Å/cycle,[33,47] and somewhat lower than for O_3 based processes, 1.1–1.2 Å/cycle.[48] However, the growth rate is close to plasma-based processes using the other alkylamide precursor TDEAH (1.1 Å/cycle).[49] The as-deposited amorphous HfO_2 proved to be nearly stoichiometric. Obtaining a stoichiometric film with ALD processes is, however, found to be not trivial, especially in the case of (partly) crystalline HfO_2 films, the existence of different crystal structures tends to lead to oxygen deficiency.[34] On the other hand, the presence of residual OH tends to lead to an oxygen excess, as has also been found earlier for amorphous Al_2O_3.[50] The uniformity seems excellent even with the relatively short plasma exposure time of 3 s compared to 10 s in the case of a H_2-N_2 plasma, which indicates that the O_2 plasma produced radicals seem less affected by the geometry of the chamber.

IV. CONCLUSIONS

The FlexAL reactor for thermal and remote plasma-assisted atomic layer depositions has been described and its main features such as plasma source, deposition chamber geometry, and precursor delivery have been discussed. Furthermore, we have demonstrated that high-quality TiN and HfO_2 films in terms of impurity contents and microstructural properties can be deposited uniformly over large substrate areas. The electrical properties of TiN based on the metal-halide process are among the state-of-the-art reported for this deposition technique at 350 °C and are comparable to results obtained on small homebuilt laboratory scale reactors. The thickness and resistivity uniformity of the TiN films were found to be $<5\%$. Furthermore, it was shown that with the same tool, an O_2 plasma-based HfO_2 process using the metal organic TEMAH precursor resulted in amorphous HfO_2 films

with low H and C contents at a deposition temperature of 290 °C. The results on HfO_2 depositions also showed that by using the same plasma source configuration to generate an O_2 plasma, a thickness uniformity within 2% can be obtained on 200 mm substrates. In the future, a more detailed investigation of the electrical properties and the conformality on substrates with a large topography will be carried out together with the exploration of new materials and deposition issues related to device processing for both remote plasma-assisted and thermal ALD. The first results on remote plasma and thermal ALD of Al_2O_3 using $Al(CH_3)_3$ dosing and O_2 plasma or H_2O exposure were promising, as will be discussed in a separate paper.[36]

ACKNOWLEDGMENTS

The authors would like to thank J. J. A. Zeebregts and M. J. F. van de Sande (Eindhoven University of Technology) and A. York and P. Burns (Oxford Instruments Plasma Technology) for their skillful technical assistance. This work is supported by the Dutch Technology Foundation STW. SenterNovem, an agency of the Netherlands Ministry of Economic Affairs is also acknowledged for its financial support in the framework of the INNOVia project. The research of one of the authors (W.M.M.K.) was made possible by a fellowship from the Royal Netherlands Academy of Arts and Sciences (KNAW).

[1]M. Ritala and M. Leskelä, in *Handbook of Thin Film Materials*, edited by H. S. Nalwa (Academic, New York, 2001), Vol. 1, p. 103.
[2]M. Tiitta and L. Niinistö, Chem. Vap. Deposition **3**, 167 (1997).
[3]E. Gerritsen *et al.*, Solid-State Electron. **49**, 1767 (2005).
[4]S. Jakschik, U. Schroeder, T. Hecht, G. Dollinger, A. Bergmaier, and J. W. Bartha, Mater. Sci. Eng., B **107**, 251 (2004).
[5]W. S. Yang, Y. K. Kim, S. Y. Yang, J. H. Choi, H. S. Park, S. I. Lee, and J. B. Yoo, Surf. Coat. Technol. **131**, 79 (2000).
[6]International Technology Roadmap for Semiconductors, Semiconductor Industry Associates, available from http://www.itrs.net (2005).
[7]A. P. Ghosh, L. J. Gerenser, C. M. Jarman, and J. E. Fornalik, Appl. Phys. Lett. **86**, 223503 (2005).
[8]M. D. Groner, S. M. George, R. S. McLean, and P. F. Carcia, Appl. Phys. Lett. **88**, 051907 (2006).
[9]G. Agostinelli, A. Delabie, P. Vitanov, Z. Alexieva, H. F. W. Dekkers, S. De Wolf, and G. Beaucarne, Sol. Energy Mater. Sol. Cells **90**, 3438 (2006).
[10]L. Reijnen, B. Meester, A. Goossens, and J. Schoonman, Chem. Vap. Deposition **9**, 15 (2003).
[11]T. T. Van and J. P. Chang, Appl. Phys. Lett. **87**, 011907 (2005).
[12]J. S. King, C. W. Neff, C. J. Summers, W. Park, S. Blomquist, E. Forsythe, and D. Morton, Appl. Phys. Lett. **83**, 2566 (2003).
[13]T. M. Mayer, J. W. Elam, S. M. George, P. G. Kotula, and R. S. Goeke, Appl. Phys. Lett. **82**, 2883 (2003).
[14]T. W. Scharf, S. V. Prasad, M. T. Dugger, P. G. Kotula, R. S. Goeke, and R. K. Grubbs, Acta Mater. **54**, 4731 (2006).
[15]Y. Won, S. Park, J. Koo, S. Kim, J. Kim, and H. Jeon, Appl. Phys. Lett. **87**, 262901 (2005).
[16]J. Kim, S. Kim, H. Jeon, M. H. Cho, K. B. Chung, and C. Bae, Appl. Phys. Lett. **87**, 053108 (2005).
[17]B. Hoex, S. B. S. Heil, E. Langereis, M. C. M. van de Sanden, and W. M. M. Kessels, Appl. Phys. Lett. **89**, 042112 (2006).
[18]H. Kim, A. J. Kellock, and S. M. Rossnagel, J. Appl. Phys. **92**, 7080 (2002).
[19]S. M. Rossnagel and H. Kim, J. Vac. Sci. Technol. B **21**, 2550 (2003).
[20]S. B. S. Heil, E. Langereis, F. Roozeboom, M. C. M. van de Sanden, and W. M. M. Kessels, J. Electrochem. Soc. **153**, G956 (2006).
[21]G. A. Ten Eyck *et al.*, Chem. Vap. Deposition **11**, 60 (2005).
[22]H. Kim, C. Cabral, C. Lavoie, and S. M. Rossnagel, J. Vac. Sci. Technol. B **20**, 1321 (2002).
[23]O. K. Kwon, S. H. Kwon, H. S. Park, and S. W. Kang, Electrochem. Solid-State Lett. **7**, C46 (2004).
[24]C. Jezewski, W. A. Lanford, C. J. Wiegand, J. P. Singh, P. I. Wang, J. J. Senkevich, and T. M. Lu, J. Electrochem. Soc. **152**, C60 (2005).
[25]ASM Genitech's tool as mentioned in S. S. Yim, M. S. Lee, K. S. Kim, and K. B. Kim, Appl. Phys. Lett. **89**, 093115 (2006).
[26]G. Lucovsky and D. V. Tsu, J. Vac. Sci. Technol. A **5**, 2231 (1987).
[27]J. Kim *et al.*, J. Appl. Phys. **98**, 094504 (2005).
[28]S. M. Rossnagel, A. Sherman, and F. Turner, J. Vac. Sci. Technol. B **18**, 2016 (2000).
[29]K. E. Elers, J. Winkler, K. Weeks, and S. Marcus, J. Electrochem. Soc. **152**, G589 (2005).
[30]K. E. Elers, T. Blomberg, M. Peussa, B. Aitchison, S. Haukka, and S. Marcus, Chem. Vap. Deposition **12**, 13 (2006).
[31]S. Kamiyama, T. Miura, and Y. Nara, Appl. Phys. Lett. **87**, 132904 (2005).
[32]M. S. Akbar, J. C. Lee, N. Moumen, and J. Peterson, Appl. Phys. Lett. **88**, 032906 (2006).
[33]K. Kukli, M. Ritala, T. Sajavaara, J. Keinonen, and M. Leskelä, Chem. Vap. Deposition **8**, 199 (2002).
[34]K. Kukli, T. Pilvi, M. Ritala, T. Sajavaara, J. Lu, and M. Leskelä, Thin Solid Films **491**, 328 (2005).
[35]P. K. Park, J. S. Roh, B. H. Choi, and S. W. Kang, Electrochem. Solid-State Lett. **9**, F34 (2006).
[36]J. L. van Hemmen, S. B. S. Heil, J. H. Klootwijk, F. Roozeboom, M. C. M. van de Sanden, and W. M. M. Kessels, J. Electrochem. Soc. **154**, G165 (2007).
[37]See EPAPS Document No. E-JVTAD6-25-004705 for a movie of the operation of the Oxford Instruments FlexAL system standing in the cleanroom at the Eindhoven University of Technology. This document can be reached via a direct link in the online article's HTML reference section or via the EPAPS homepage (http://www.aip.org/pubservs/epaps.html).
[38]E. Langereis, S. B. S. Heil, M. C. M. van de Sanden, and W. M. M. Kessels, J. Appl. Phys. **100**, 023534 (2006).
[39]S. B. S. Heil, E. Langereis, A. Kemmeren, F. Roozeboom, M. de Sanden, and W. M. M. Kessels, J. Vac. Sci. Technol. A **23**, L5 (2005).
[40]S. B. S. Heil, P. Kudlacek, E. Langereis, R. Engeln, M. C. M. van de Sanden, and W. M. M. Kessels, Appl. Phys. Lett. **89**, 3 (2006).
[41]Y. J. Lee and S. W. Kang, J. Vac. Sci. Technol. A **21**, L13 (2003).
[42]A. C. Dillon, M. L. Wise, M. B. Robinson, and S. M. George, J. Vac. Sci. Technol. A **13**, 1 (1995).
[43]A. Rahtu and M. Ritala, J. Mater. Chem. **12**, 1484 (2002).
[44]K. Kukli *et al.*, J. Appl. Phys. **96**, 5298 (2004).
[45]M. J. Biercuk, D. J. Monsma, C. M. Marcus, J. S. Becker, and R. G. Gordon, Appl. Phys. Lett. **83**, 2405 (2003).
[46]K. Kukli *et al.*, Thin Solid Films **479**, 1 (2005).
[47]D. W. McNeil (private communication).
[48]S. Kamiyama, T. Miura, and Y. Nara, Electrochem. Solid-State Lett. **8**, F37 (2005).
[49]J. Choi, S. Kim, J. Kim, H. Kang, H. Jeon, and C. Bae, J. Vac. Sci. Technol. A **24**, 678 (2006).
[50]E. Langereis, M. Creatore, S. B. S. Heil, M. C. M. Van de Sanden, and W. M. M. Kessels, Appl. Phys. Lett. **89**, 081915 (2006).